Copyright 2019 Society of Photo-Optical Instrumentation Engineers (SPIE).

One print or electronic copy may be made for personal use only. Systematic reproduction and distribution, duplication of any material in this publication for a fee or for commercial purposes, and modification of the contents of the publication are prohibited.

Bekir Aksoy, Herbert Shea, "Dynamically reconfigurable DEAs incorporating shape memory polymer fibers ," Proc. SPIE 10966, Electroactive Polymer Actuators and Devices (EAPAD) XXI, 109661Y (13 March 2019); doi: 10.1117/12.2513195

https://doi.org/10.1117/12.2513195

PROCEEDINGS OF SPIE

SPIEDigitalLibrary.org/conference-proceedings-of-spie

Dynamically reconfigurable DEAs incorporating shape memory polymer fibers

Bekir Aksoy, Herbert Shea

Bekir Aksoy, Herbert Shea, "Dynamically reconfigurable DEAs incorporating shape memory polymer fibers ," Proc. SPIE 10966, Electroactive Polymer Actuators and Devices (EAPAD) XXI, 109661Y (13 March 2019); doi: 10.1117/12.2513195

SPIE.

Event: SPIE Smart Structures + Nondestructive Evaluation, 2019, Denver, Colorado, United States

Downloaded From: https://www.spiedigitallibrary.org/conference-proceedings-of-spie on 18 Jun 2023 Terms of Use: https://www.spiedigitallibrary.org/terms-of-use

Dynamically reconfigurable DEAs incorporating shape memory polymer fibers

Bekir Aksoy and Herbert Shea
Soft Transducers Laboratory (LMTS), Ecole Polytechnique Fédérale de Lausanne (EPFL),
CH-2000 Neuchâtel, Switzerland

ABSTRACT

We present variable stiffness dielectric elastomer actuators (DEAs), combining a single DEA actuator with embedded shape memory polymer (SMP) fibers, which can be electrically addressed to locally reduce the stiffness by a factor of 100. The device accommodates two SMP fiber sets oriented perpendicularly on both sides of a DEA, which enables a selective deformation in two different directions. During electrostatic actuation, one of the SMP fiber sets is softened by Joule heating, whereas the unaddressed fiber set remains stiff and determines the actuation direction, principally along the direction of the soft fibers. Using SMPs as a latching mechanism allows holding a given actuated position without any power, which leads to much longer lifetime in static (DC) conditions. The DEA is made of a prestretched acrylic elastomer (VHB, 3M) sandwiched between carbon-loaded polydimethylsiloxane electrodes providing an active area of 20 mm x 20 mm. The SMP fibers are electrically isolated from the DEA electrodes using 40 μm thick acrylic elastomer films. Each SMP fiber is 100 μm thick, 750 μm wide and is on a 6 mm pitch. The ratio of locked strains in the direction of the heated and the unheated fibers is measured to be 1.80 for a square DEA. This ratio is increased up to 8 with a cross-shape DEA using only two variable width fibers, one aligned vertically and the other horizontally.

Keywords: Variable stiffness DEAs, DEA modeling for strain locking, reconfigurable DEAs, shape memory polymers

1. INTRODUCTION

Dielectric elastomer transducers combine a simple structure with high energy density, fast response, and high strain capabilities [1]. Improved design and materials have led to increased actuation performance and to improved load-bearing capacity, for instance by incorporating stiff fibers [2-4], using bistable electroactive polymers as dielectric elastomers [5-7], and integrating flexible but inextensible frames [8-10].

Stiff fibers embedded in or on dielectric elastomer reinforce the membrane along the fiber direction and thereby enhance the electrically-induced deformation in the transverse direction. Fiber-constrained DEAs enable us i) to obtain high unidirectional actuation strain and, ii) to predetermine the actuation direction. The number of fibers and their orientations result in different deformation shapes. For example, Shian *et al.* demonstrated how different deformation shapes can be obtained with different fibers configurations [11].

Variable stiffness materials enable morphological shape change while maintaining structural strength and can reversibly alternate between load-bearing and flexible states. This is a promising approach that can be adapted in DEA applications. Technologies based on particle jamming, electrorheological fluids, shape memory polymers (SMP) and low-melting-point alloys have been developed for this purpose. Integrating variable stiffness materials with DEAs generally increases the complexity of the overall structure and reduces the actuation strain. Low-melting-point alloys and conductive SMPs are appealing as the phase change can be obtained by direct Joule heating, allowing for simple electrical control [12, 13]. DEAs taking advantage of this combination have been shown to withstand relatively higher loads [12, 13]. Bistable electroactive polymers offer an alternative to dielectric membranes that combine the electrically-induced actuation of dielectric elastomers and bistable deformation of shape memory polymers [6]. These materials can find applications in tactile displays, adaptive structures, and bio-inspired soft robots [14].

DEAs have an actuation direction and shape that is defined by the boundary conditions and by any embedded stiff fibers. These conditions are imposed when the device is assembled and cannot be changed during device operation. Here, we overcome this limitation by integrating DEAs with SMP fibers. We demonstrate that DEAs can be dynamically

Electroactive Polymer Actuators and Devices (EAPAD) XXI, edited by Yoseph Bar-Cohen, Iain A. Anderson,
Proc. of SPIE Vol. 10966, 109661Y · © 2019 SPIE · CCC code: 0277-786X/19/$18 · doi: 10.1117/12.2513195

Downloaded From: https://www.spiedigitallibrary.org/conference-proceedings-of-spie on 18 Jun 2023
Terms of Use: https://www.spiedigitallibrary.org/terms-of-use

reconfigured to actuate in different directions and they can be latched in any actuated state. We use thermoplastic polyurethane shape memory polymers. Their stiffness changes by two orders of magnitude with small temperature fluctuations around its glass transition region. They have high shape fixity ratio.

2. DESIGN CONCEPT AND WORKING MECHANISM

2.1 Design concept

The presented device combines a single DEA between two perpendicular SMP fiber sets (see Fig. 1a). During actuation, one of the SMP fiber sets is softened by Joule heating, while the other one remains stiff and determines the direction of voltage-induced deformation. Fibers are made of conductive SMPs and the electrical connections to them are made by pad-printed silicone electrodes. Two passive elastomer layers are placed between fiber sets and DEA electrodes for electrical insulation. These layers also serve as thermal insulation between addressed and unaddressed fibers. Each fiber sets has 4 SMP fibers which are optimized for minimum cross-heating using finite element modeling (FEM). The cross-section of each fiber is optimized for both actuation and latching states using an analytical model.

2.2 Fabrication details

The fabrication starts by prestretching of acrylic elastomer (VHB 4905 from 3M) and fixing it to a rigid PMMA frame. Compliant electrodes based on mixture of carbon-black (Ketjenblack EC-600JD from Akzo Nobel N.V.) and polydimethylsiloxane (Silbione LSR 4305 from Elkem Silicones) are then pad-printed on the prestretched membrane using a mask for patterning [15]. This stack is put in an oven at 80 °C for 1 hour to cure the electrodes. After curing, two insulation layers of thickness 40 μm (467MP from 3M) are placed on both sides. For shape memory polymers, we use thermoplastic polyurethane (SMP MM4520 from SMP Technologies Inc.). The conductive SMP layers are fabricated separately and then assembled on the DEA. The fabrication process of SMP MM4520 was developed in our lab for flexible haptic devices and microfluidic valves [16, 17]. MM4520 comes in pellets form. These pellets are dissolved in a container with dimethylformamide (DMF) at a weight ratio of 1:4 at 80 °C for 12 hours. In another container, carbon-black is ball-mixed with DMF at a weight ratio of 1:20 at 2000 rpm for 5 minutes. The solutions in these two containers are then ball-mixed together for 5 minutes at 2000 rpm. This mixture is blade-casted on a PET sheet that was covered with a sacrificial layer of Teflon. To evaporate the DMF, a programmable hot plate is used (for 4 h with positive and negative ramps of 60 °C/h from 20 °C to 80 °C and a plateau of 4 h at 80 °C). After this, the conductive SMP membrane is cured, it is shaped in fiber form using a laser cutter. The SMP fibers are transferred onto insulation layers with 90° of alignment between top and bottom fibers. Thanks to stickiness of 467MP, no further surface treatment is required for this process. For electrical connection between these fibers and metal contacts, polydimethylsiloxane mixed with carbon particle is pad-printed on both sides. The whole stack is finally cured at 80 °C for 1 h.
The assembled device is shown in Fig. 1b. The device has 6 electrical connections, two of which are used for electrostatic actuation of DEA. The remained 4 connections are used to apply voltage for heating top and bottom SMP fibers.

2.3 Working principle

Figure 1c shows the steps for actuation along the *y*-axis. The first step is to soften fibers that are aligned in *y*-direction by applying voltage (V_{JH}) through the top electrodes. This increases the temperature of SMP fibers above their glass transition region. Once fibers are heated, a high voltage is applied to the DEA electrodes. To lock the device in this actuated state, we first remove the heating voltage while keeping the DEA voltage applied for an additional 30s. After this shape fixation, we remove the DEA voltage. Thanks to shape memory ability of polyurethane, we can keep the device in actuated state even after high voltage is removed. To recover this deformation we simply reheat the same fibers. A similar approach can be repeated to actuate and to lack the device in *x*-direction by electrically addressing the fibers in *x*-axis.

Downloaded From: https://www.spiedigitallibrary.org/conference-proceedings-of-spie on 18 Jun 2023
Terms of Use: https://www.spiedigitallibrary.org/terms-of-use

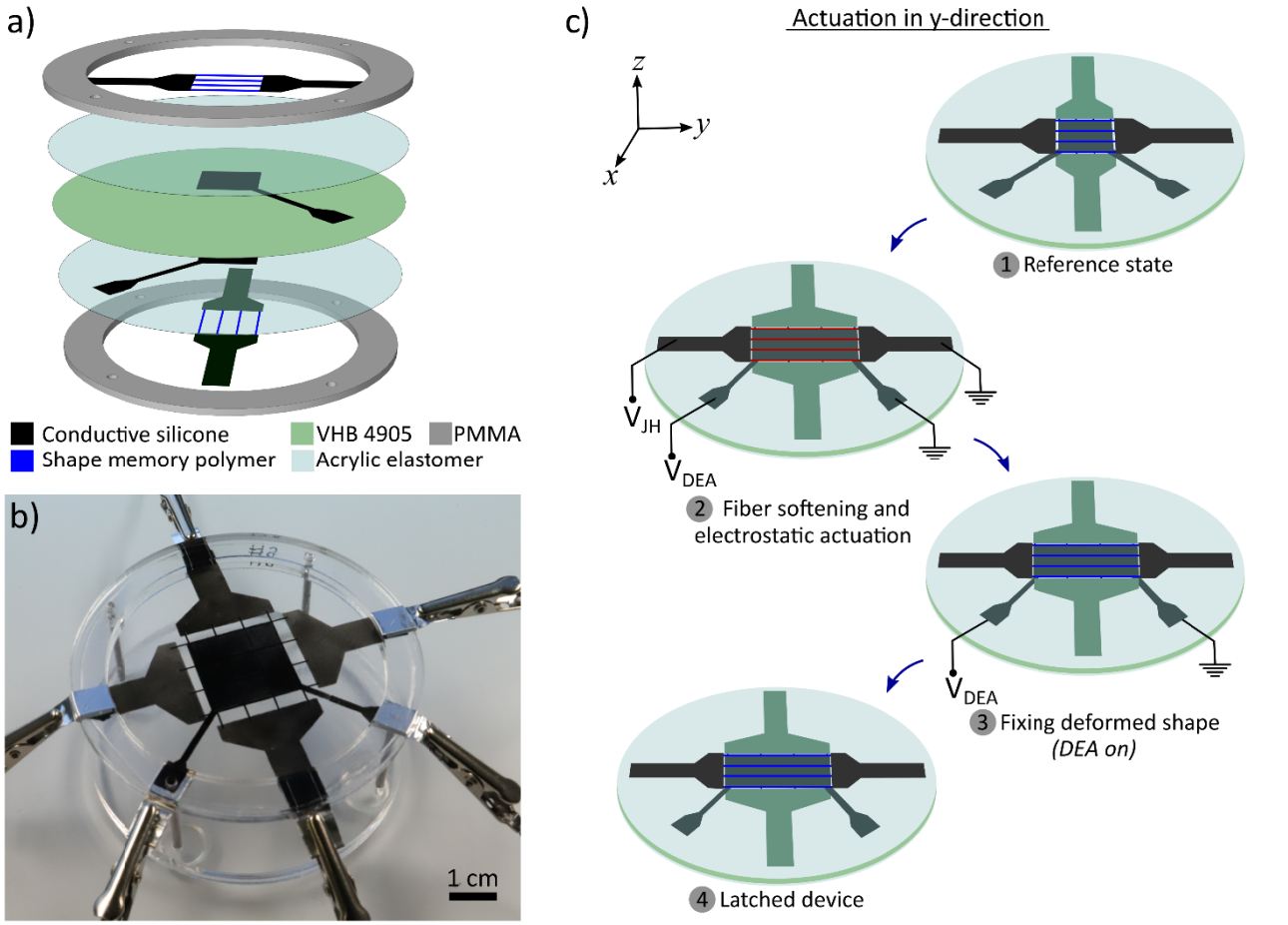

Figure 1. a) Exploded view of a DEA with 2 perpendicular sets of conductive SMP fibers b) Photograph of an assembled device showing electrical connections to the DEA and to the conductive SMP fibers. The DEA has an active area of 20 mm x 20 mm. c) Steps to actuate and to latch the device in the *y*-direction. The actuation direction is determined by bottom SMP fibers which remain stiff during the electrostatic actuation. Actuation in the *x*-direction is achieved by heating the bottom fibers and keeping the top fibers cool.

3. OPTIMIZATION OF DESIGN PARAMETERS USING FEM AND ANALYTICAL MODELS

Our device takes advantage of the large change in Young's modulus of SMPs when heated above its glass transition temperature. Soft SMPs enable us to achieve reasonable actuation strain. Stiff SMPs lock in the actuation strain, the locked strain. The temperature dependence of the Young's modulus of SMP MM4520 is measured by dynamic mechanical analysis (DMA). The red curve in Fig. 2 shows the Young's modulus of bare SMP as a function of temperature. At room temperature it has a Young's modulus of 2 GPA and above 75 °C this decreases to 20 MPa. We made the SMP conductive by adding carbon particles. Compared to adding a heating layer, using conductive SMPs reduces the number of layers in the device and simplifies the fabrication process. Figure 2 compares the Young's moduli of bare SMP and carbon-loaded SMP membranes.

Downloaded From: https://www.spiedigitallibrary.org/conference-proceedings-of-spie on 18 Jun 2023
Terms of Use: https://www.spiedigitallibrary.org/terms-of-use

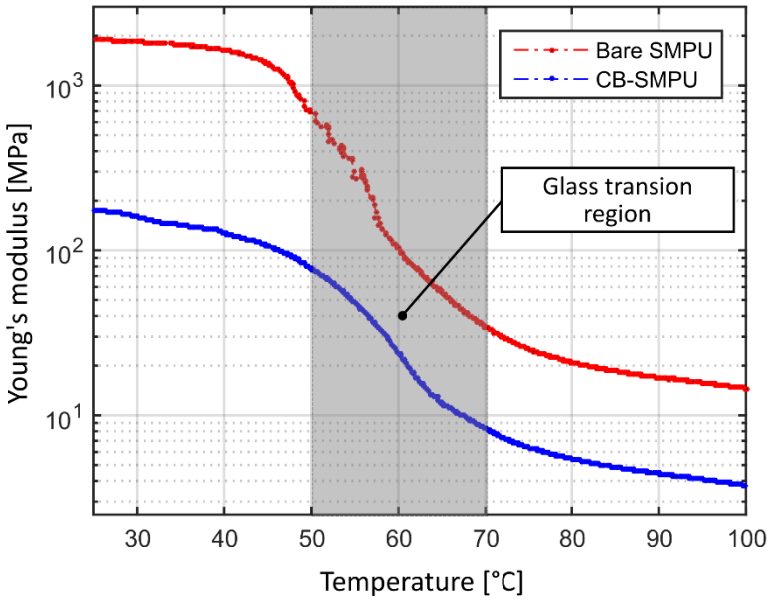

Figure 2. The Young's moduli of bare SMP and carbon-loaded SMP as functions of temperature

3.1 Finite Element Model for thermal analysis

The performance of the device depends on how well the heated and the unheated fibers are thermally decoupled. We use finite element models to design a device that minimizes the amount of the heat transferred between the fiber sets. The parameters that we optimize in these models are the thickness of the passive layers and the number of the fibers.

The goal of the first FEM (COMSOL Multiphysics®) simulation is to investigate the effect of insulation layer thickness on cross-heating. The model includes all components that are shown in Fig. 1a. The dielectric membrane constructed in the model has a diameter of 60 mm and a thickness of 35 µm. The DEA electrodes have thicknesses of 5 µm with a square area of 20 mm x 20 mm and they are placed on the top and bottom of the dielectric membrane. Insulation layers cover these electrodes and their initial thickness is 25 µm. In this simulation, we use 2 fiber sets each of which consists of 4 fibers (75 µm x 100 µm x 25 mm). They are aligned perpendicularly on the bottom and top of the insulation layers. The thermal conductivity of the dielectric membrane and the passivation layers used in this model is 0.19 W/mK. The carbon-loaded membranes, SMP and PDMS, are expected to have higher thermal conductivity; we use 2 W/mK for those membranes. The heat capacities of the dielectric membrane and the passivation layer is taken to be 1460 J/kg.K. The heat capacities of the PDMS and SMP membranes are 1380 and 1900 J/kg.K. A heating voltage is applied to the top fibers. Then we plot the temperature distribution along the top fibers and the bottom fibers (see Fig. 3a). This procedure is repeated for different insulation layer thicknesses, from 25 µm to 100 µm.

Figure 3b plots the temperature distribution across the heated and unheated fibers for two different insulation layer thicknesses: 25 µm and 100 µm. The addressed fibers have a uniform temperature distribution, slightly decreasing at overlaps between the heated and unheated fibers. Unaddressed fibers, on the other hand, have a varying temperature profile; highest at the overlaps. As the thickness of the insulation layer increases, the temperature of the unheated fibers at the overlaps slightly decreases. Numerically, increasing the insulation layer thickness from 25 µm to 100 µm, decreases the temperature of the unheated fibers by 2 °C at the overlaps. On the other hand, thicker membranes cannot dissipate heat into air as fast as thinner ones. This allows heat to transfer in lateral direction which increases the temperature of the unheated fibers in regions outside the overlaps. These simulations show that 100 µm thick insulation layers do not efficiently prevent the heat transfer between fibers.

The second FEM simulation compares how the number of fibers changes the temperature distribution across the unheated fibers. For this simulation, we keep the thickness of the insulation layer as 25 µm and vary the number of

Downloaded From: https://www.spiedigitallibrary.org/conference-proceedings-of-spie on 18 Jun 2023
Terms of Use: https://www.spiedigitallibrary.org/terms-of-use

fibers. Figure 3c shows the FEM results for devices with 4-fibers and 6-fibers. The overall temperature of the unheated fibers increases with the number of fibers due to the total increase of overlap areas. Finite element models show that the heat transfer between fiber sets can be reduced 1) using fewer fibers per set and 2) using thinner insulation layers. Our design uses 4 SMP fibers per set, the minimum number that can provide a uniform strain distribution across an active area of 20 mm x 20 mm, and insulation layers with a thickness of 40 µm. Figure 3d shows the experimental results of this device (thermal imaging with a FLIR A15 from FLIR systems, Inc.). As previously seen from the FEM results, we have a uniform temperature across the heated fibers and a varying temperature on the unheated fibers.

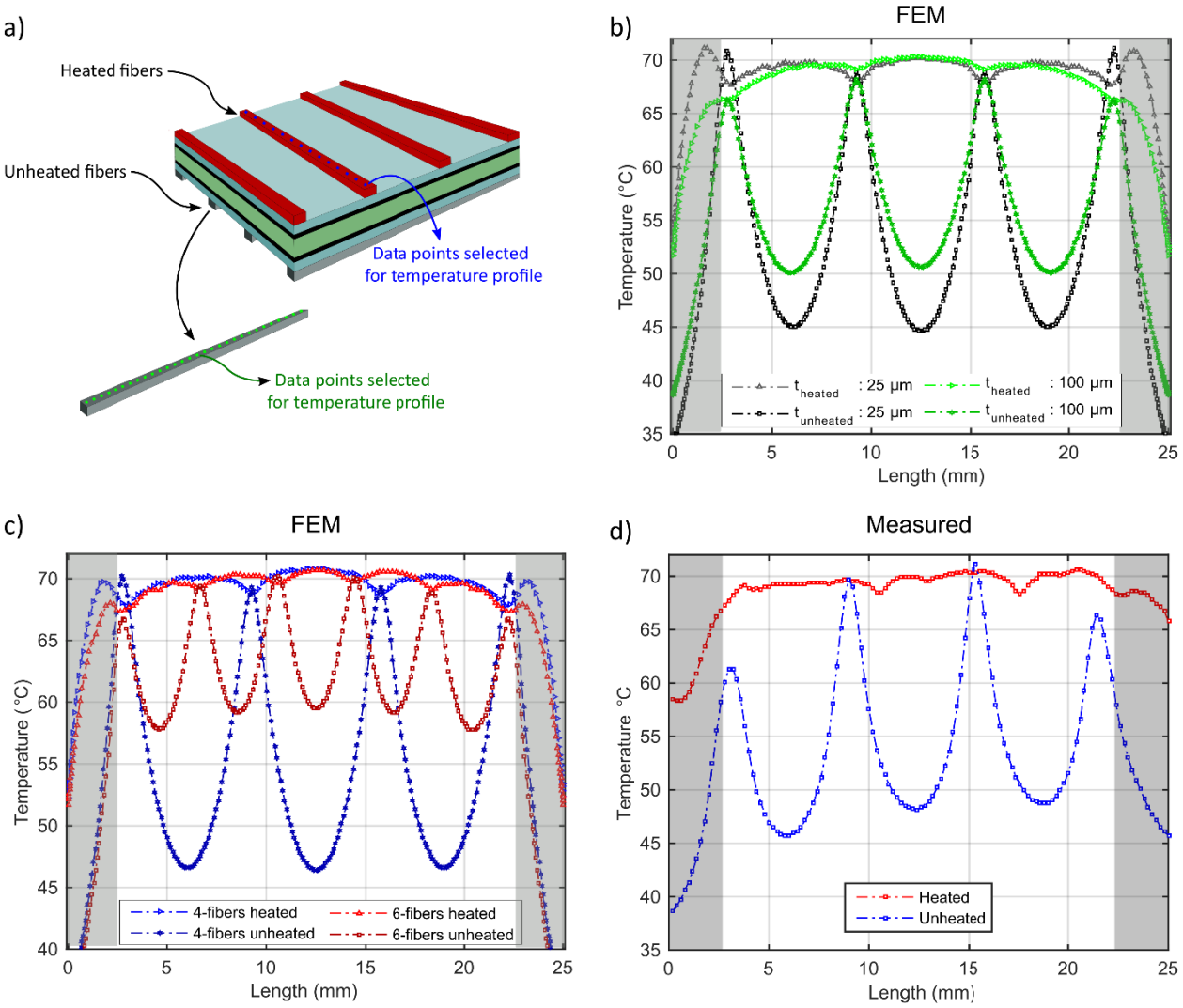

Figure 3. a) The schematic of the DEA illustrating where we take the temperature profiles for the heated and the unheated fibers. b) Simulated temperature distribution across the length of the heated and the unheated fibers for 25 µm (black) and 100 µm (green) thick insulation layers. c) The temperature profile of heated and unheated fibers for devices with 4 (blue) and 6 (red) fibers. d) Experimentally obtained temperature profiles for heated and unheated fibers.

3.2 Analytical modeling of DEAs for actuation and locked strains

Actuation and locked strains favor different fiber cross-sections: thin SMP fibers have less stiffening impact on the actuation strain but they are weak to lock the actuation strain. Thick SMP fibers, however, significantly reduce actuation strain but it can lock most of this strain. Our analytical models aims to find best trade-off between actuation and locked strains.

Downloaded From: https://www.spiedigitallibrary.org/conference-proceedings-of-spie on 18 Jun 2023
Terms of Use: https://www.spiedigitallibrary.org/terms-of-use

DEAs are generally modeled based on the stress equilibrium of the dielectric membrane; the stiffening impact of electrodes are neglected. The scale of this stiffening depends on the Young's modulus of electrodes and their thickness. If both the elastic modulus and the thickness are lower than the dielectric material, this stiffening effect can be ignored. Otherwise, the stiffening should be taken into account [18]. In our design, we have multiple layers and each layer has a comparable thickness and stiffness (see close-ups in Fig. 4). Thus, we consider the effect of these layers in our calculation. We use equations for force equilibrium instead of stress equilibrium. The stress generated in the membranes are converted into force by multiplying the stress value with cross-sectional areas on which it acts.

Table 1 shows the stretch values and the cross-sectional areas of all membranes in different states. These are the values in the direction of actuation. We assume that there is no deformation in the perpendicular direction. This table helps to understand how the membranes deforms and also how the cross-section areas change in these states. As seen from the table, each membrane has different stretch values. This is due to the fact that VHB is prestretched and the SMP fibers fix their shape upon cooling. For example, the total stretch of the VHB in the actuated state is $\lambda_{pre}\,\lambda_{act}$, whereas the total stretch of the insulation layers is λ_{act}. Upon cooling, the stretch values of the VHB and the insulation layers remain the same but the stretch value of the SMP fibers goes from λ_{act} to 1. This enables us to lock in the actuation strain.

The initial thickness of all membranes and their cross-sectional areas are known. As the membranes undergoes different states, the thicknesses and the cross-section areas change. Although there are many parameters listed in the table, the only unknowns are λ_{act} and λ_{cont} which stand for the actuation stretch and the contraction value. Thus, we need two equations from two different states: one from the actuation state and the other one from the latched state.

Table 1: Stretch values and cross-sectional area of membranes for different states.

	Reference state		Actuated state (heating on)		Actuated state (heating off)		Latched state	
	Stretch value	Cross-section, A	Stretch value, λ_{1a}	Cross-section, A	Stretch value	Cross-section, A	Stretch value, λ_{1f}	Cross-section, A
VHB 4905	λ_{pre}	$\frac{L_{0v}T_{0v}}{\lambda_{pre}^2}$	$\lambda_{pre}\lambda_{act}$	$\frac{L_{0v}T_{0v}}{\lambda_{pre}^2\lambda_{act}}$	$\lambda_{pre}\lambda_{act}$	$\frac{L_{0v}T_{0v}}{\lambda_{pre}^2\lambda_{act}}$	$\lambda_{pre}\lambda_{act}\lambda_{cont}$	$\frac{L_{0v}T_{0v}}{\lambda_{pre}^2\lambda_{act}\lambda_{cont}}$
467MP	1	$L_{0i}T_{0i}$	λ_{act}	$\frac{L_{0i}T_{0i}}{\lambda_{act}}$	λ_{act}	$\frac{L_{0i}T_{0i}}{\lambda_{act}}$	$\lambda_{act}\lambda_{cont}$	$\frac{L_{0i}T_{0i}}{\lambda_{act}\lambda_{cont}}$
SMP fibers (soft)	1	$W_{f}T_{f}$	λ_{act}	$\frac{W_{f}T_{f}}{\lambda_{act}}$	1	$\frac{W_{f}T_{f}}{\lambda_{act}}$	λ_{cont}	$\frac{W_{f}T_{f}}{\lambda_{act}\lambda_{cont}}$

Figure 4 shows the reference state, where only the dielectric is biaxially prestretched while all other components are at rest. The DEA is then actuated by simultaneously applying Joule heating and electrostatic actuation (see the 2nd state in Fig. 4). In the actuated state, the elasticity of the elastomers is balanced by the stress due to mechanical prestretch and by the Maxwell stress due to electrostatic interaction. We use the Gent hyperelastic material model for strain energy density function [19]. We assume that the deformation is completely uniaxial. Adapting the methodology of [2] to our case, the equilibrium of the forces in the direction of the elongation can be written as follow:

$$A_{pre}\varepsilon\sigma_{pre}+A_v\varepsilon E^2 = A_v\frac{\mu_v\left(\lambda_{1v}^2-\lambda_{1v}^{-2}\lambda_{2v}^{-2}\right)}{1-\left(\lambda_{1v}^2+\lambda_{2v}^2+\lambda_{1v}^{-2}\lambda_{2v}^{-2}-3\right)/J_v}+2A_i\frac{\mu_i\left(\lambda_{1i}^2-\lambda_{1i}^{-2}\lambda_{2i}^{-2}\right)}{1-\left(\lambda_{1i}^2+\lambda_{2i}^2+\lambda_{1i}^{-2}\lambda_{2i}^{-2}-3\right)/J_i}+N_sA_s\frac{\mu_s\left(\lambda_{1s}^2-\lambda_{1s}^{-2}\lambda_{2s}^{-2}\right)}{1-\left(\lambda_{1s}^2+\lambda_{2s}^2+\lambda_{1s}^{-2}\lambda_{2s}^{-2}-3\right)/J_s} \quad (1)$$

where λ_1, λ_2, μ, J, E, A, N, and ε are the principle stretches in the directions of the heated and the unheated fibers, the shear modulus, the limiting stretch of membranes, the applied electric field, the cross-sectional area, the number of fibers in one set, and the dielectric constant, respectively. Subscripts *pre, a, v, i, s* stand for prestretch, actuation, VHB,

Downloaded From: https://www.spiedigitallibrary.org/conference-proceedings-of-spie on 18 Jun 2023
Terms of Use: https://www.spiedigitallibrary.org/terms-of-use

insulation layer, and SMP fibers. The first term of the left-hand side is the force generated by the mechanical prestretch and it is assumed to be constant for all states. The second term of the left-hand side is the force caused by electrostatic actuation of dielectric membrane. Three terms on the right-hand side of the equations represent the forces generated due to deformations of VHB 4905, MP467, and SMP fibers. As we assume that the deformation is completely constrained in the direction of the stiff fibers (direction 2 in this care), we can substitute the following equations in Eq. 1: $\lambda_{2v} = \lambda_{pre}$, $\lambda_{2i} = 1$, and $\lambda_{2s} = 1$. By substituting the stretch values in the actuation direction that are listed in Table 1, we simplify Eq.1 as:

$$A_{pre}\sigma_{pre} + A_v\varepsilon E^2 = A_v \frac{\mu_v\left(\lambda_p^2\lambda_a^2 - \lambda_p^{-4}\lambda_a^{-2}\right)}{1-\left(\lambda_p^2\lambda_a^2 + \lambda_p^2 + \lambda_p^{-4}\lambda_a^{-2} - 3\right)/J_v} + 2A_i \frac{\mu_i\left(\lambda_a^2 - \lambda_a^{-2}\right)}{1-\left(\lambda_a^2 + 1 + \lambda_a^{-2} - 3\right)/J_i} + N_s A_s \frac{\mu_i\left(\lambda_a^2 - \lambda_a^{-2}\right)}{1-\left(\lambda_a^2 + 1 + \lambda_a^{-2} - 3\right)/J_s} \quad (2)$$

The shear moduli of the VHB and the insulation layers (467MP) are found using $\mu = E/2(1+\nu)$, where E is the Young's modulus and ν is the Poisson's ratio. The Young's moduli are found to be 63 kPa and 44 kPa using a uniaxial tensile test. The limiting stretch for both of these membranes is taken as 120. For the conductive SMP fibers, DMA is carried out to measure Young's modulus as a function of temperature. The results of the DMA are summarized in Fig. 2a. For the actuation model, we use shear modulus of the SMP in the rubbery state. The active region of the DEA has a square area of 20 mm x 20 mm (L_0 = 20 mm). The initial thicknesses of VHB 4905 and MP467 are 500 µm and 60 µm.

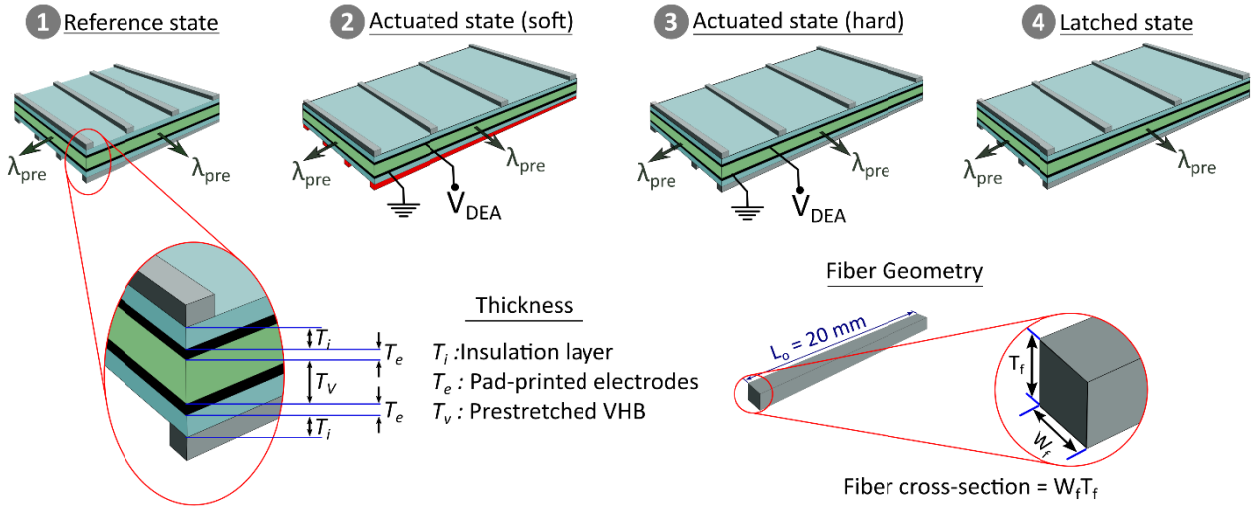

Figure 4. Schematic illustration of different states of the device modeled analytically.

The model includes two failure modes of DEA: dielectric breakdown and electromechanical instability (see Figure 5a) [20-22]. The dielectric strength of VHB is taken as 250 V/µm. As the electric field in the dielectric elastomer increases, it gets thinner so that the same voltage induces even higher electric field. This positive feedback between the thinning of membrane and the increasing of electric field is known as the electromechanical instability. Figure 5a plots the applied voltage as a function of the total stretch of VHB and shows the regions where failures occur. Solid parts of the lines represent the safe region of operation, whereas the dashed parts of the lines shows the region where the device fails.

Downloaded From: https://www.spiedigitallibrary.org/conference-proceedings-of-spie on 18 Jun 2023
Terms of Use: https://www.spiedigitallibrary.org/terms-of-use

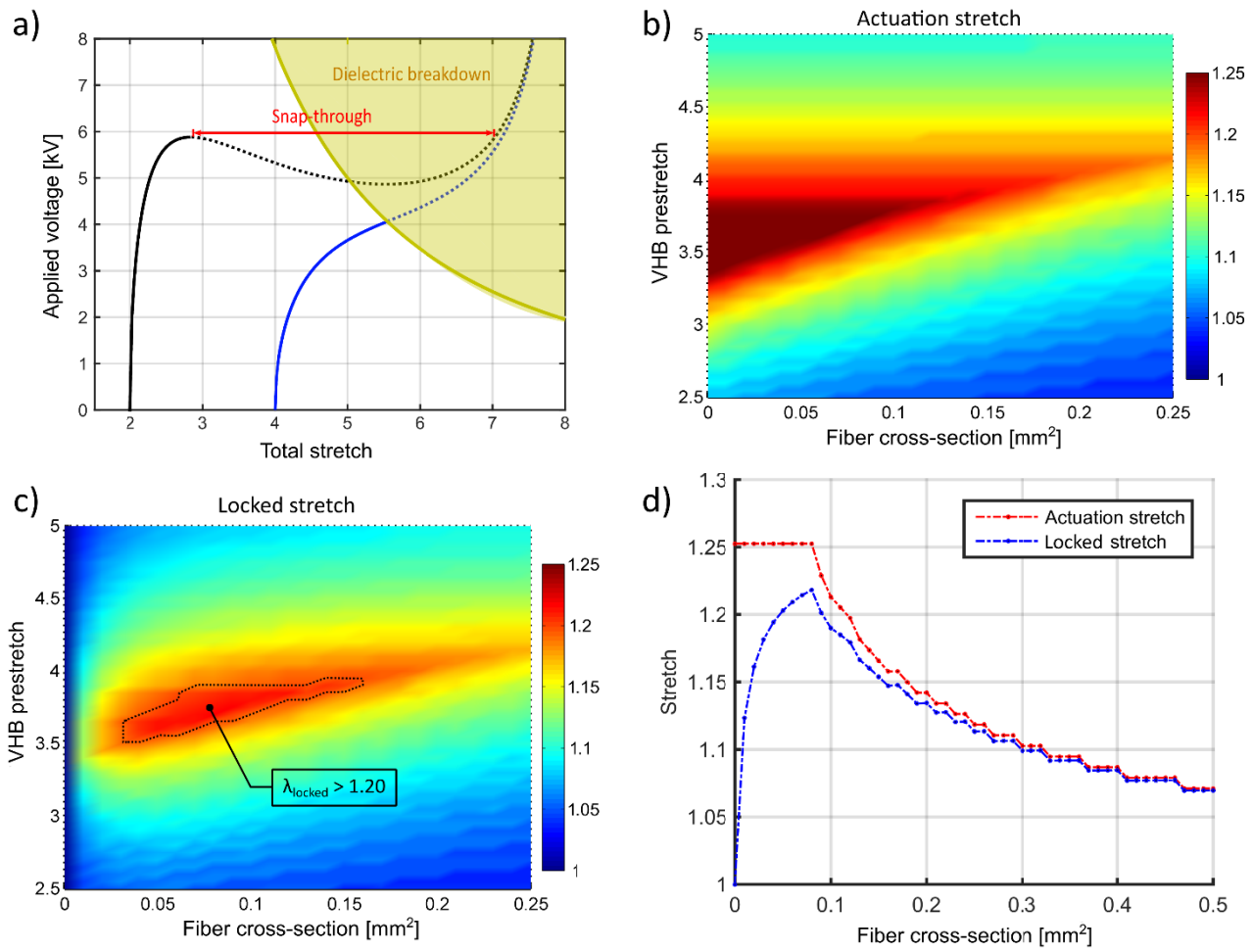

Figure 5. Output of the analytical model. a) Plot of applied voltage vs. total elastomer stretch, showing dielectric breakdown and snap-through regions. b) and c) Surface plots of the actuation and the locked stretches as a function of cross-sectional area of SMP fibers and VHB prestretch. The region with $\lambda_{locked} > 1.20$ is enclosed with dashed lines. d) The actuation and the locked stretches for a prestretch of 3.70. The maximum actuation stretch at smaller cross-sections is limited by the dielectric breakdown, whereas at larger cross-section it is limited by 5 kV power supply.

Using Eq. 2 with the constraints mentioned above, we plot the actuation stretch as a function of VHB prestretch and fiber cross-section (see Fig. 5b). The actuation stretch for any prestretch is at its maximum where the cross-sectional area of SMP is zero (no fibers). As the cross-section of the fibers increases, the actuation strain decreases. To find the optimum cross-section that enables maximum locked strain, we developed an analytical model for the latching part. In the latched state, the deformation is locked by the SMP fibers: the VHB and the insulation layers want to shrink down as they do not have a shape memory effect. The SMP fibers, on the other hand, keep their deformed shapes and oppose this contraction. The equilibrium of this state can be written as follow:

$$A_{pre}\sigma_{pre} = A_v \frac{\mu_v\left(\lambda_{1fv}^2 - \lambda_{1fv}^{-2}\lambda_{2fv}^{-2}\right)}{1-\left(\lambda_{1fv}^2 + \lambda_{2fv}^2 + \lambda_{1fv}^{-2}\lambda_{2fv}^{-2} - 3\right)/J_v} + 2A_i \frac{\mu_i\left(\lambda_{1fi}^2 - \lambda_{1fi}^{-2}\lambda_{2fi}^{-2}\right)}{1-\left(\lambda_{1if}^2 + \lambda_{2fi}^2 + \lambda_{1fi}^{-2}\lambda_{2fi}^{-2} - 3\right)/J_i} + N_s A_s \frac{\mu_s\left(\lambda_{1fs}^2 - \lambda_{1fs}^{-2}\lambda_{2fs}^{-2}\right)}{1-\left(\lambda_{1fs}^2 + \lambda_{2fs}^2 + \lambda_{1fs}^{-2}\lambda_{2fs}^{-2} - 3\right)/J_s} \quad (3)$$

where subscript *f* stands for the final stretch of membranes. When we plug in the final stretch values listed in the last column of Table 1, we reduce the number of unknowns in Eq. 3 as follow:

Downloaded From: https://www.spiedigitallibrary.org/conference-proceedings-of-spie on 18 Jun 2023
Terms of Use: https://www.spiedigitallibrary.org/terms-of-use

$$A_{pre}\sigma_{pre} = A_v \frac{\mu_v\left(\lambda_p^2\lambda_a^2\lambda_c^2 - \lambda_p^{-4}\lambda_a^{-2}\lambda_c^{-2}\right)}{1-\left(\lambda_p^2\lambda_a^2\lambda_c^{-2} + \lambda_p^2\lambda_c^{-2} + \lambda_p^{-4}\lambda_a^{-2}\lambda_c^{-2} - 3\right)/J_f} + 2A_i \frac{\mu_i\left(\lambda_a^2\lambda_c^2 - \lambda_a^{-2}\lambda_c^{-2}\right)}{1-\left(\lambda_a^2\lambda_c^2 + \lambda_c^2 + \lambda_a^{-2}\lambda_c^{-2} - 3\right)/J_i} + N_S A_S \frac{\mu_i\left(\lambda_c^2 - \lambda_c^{-2}\right)}{1-\left(\lambda_c^2 + 1 + \lambda_c^{-2} - 3\right)/J_S} \quad (4)$$

where λ_c is the ratio of shrink after the DEA voltage is removed. λ_C can be quantified as the ratio of the final stretch to the actuation stretch. Figure 5c shows the surface plot of the holded stretch. Depicted from this plot, one can observe the effect of the cross-section of the SMP on the actuation and the holded stretches. If the cross-section of the SMP fibers are too small or too big then the holded stretch is lower. This is because very small cross-sections do not resist to membranes contraction upon cooling and very large cross-sections introduce more stiffening effect on the actuation which eventually reduces the final stretch. A region with $\lambda_{locked}>1.20$ is outlined in Fig. 5c. This region gives us a range of prestretch values and fiber cross-sectional areas where we can achieve locked strain greater than 20% and we select our design parameters accordingly. Figure 5d shows the actuation and locked stretches plotted for VHB prestretch of 3.70 where the maximum locked stretch is achievable. The actuation stretch in this graph has a plateau in smaller cross-sectional areas. The maximum actuation stretch in this region is limited by dielectric breakdown. For larger cross-sectional areas (>0.075 mm^2), however, the maximum actuation stretch is limited by power supply (we use a 5 kV power supply for the DEA actuation).

4. EXPERIMENTAL RESULTS AND DISCUSSION

Figure 6a shows the time sequence of the Joule heating and the DEA voltages that are applied to achieve actuation in the *x* and then in the *y*-directions. The actuation starts with simultaneous applying DEA and heating voltages using a 5kV and 240 V power supply [23]. After the DEA and the SMP fibers are simultaneously actuated for 30 seconds, the heating voltage is removed while the DEA actuation is kept on for additional 30 s to provide time to cool down the membrane and thus to lock in the deformed shape. The device is then held latched for 1 min with no applied voltage. To go back to the reference state, we apply a heating voltage to the SMP fibers for 15s. The same procedure is then followed to get actuation in the perpendicular direction by softening the other SMP fibers. To measure the evolution of in-plane strain components, images of deformed membranes are captured at a frequency of 1 Hz. The deformed images are processed using digital image correlation method [24].

Figure 6b shows the evolution of the in-plane strains as the DEA is actuated in *y* and then in *x* directions. The highest strain is achieved in the direction of the softened SMP fibers. However, a significant amount of deformation takes place in the transverse direction due to cross-heating between the addressed and the unaddressed SMP fibers. Panel c of Fig. 6 shows strain mapping of the in-plane components at t = 280s. The warmer colors represent higher strain amplitudes whereas the cooler colors show lower strain values. The strain distribution is not completely uniform. This is mostly due to non-uniform heating and fabrication imperfections. The fibers heated the most will have the highest actuation strain.

A polymer under a constant tensile force shrinks upon heating and expands upon cooling. This is due to elasticity increase through entropic straightening of polymer chains, followed by recoiling into a conformation of maximum entropy. This phenomenon is the Gough-Joule effect [25]. Per actuation cycle, we observe this twice: first when we remove the heating voltage, and second when we apply heating to go back to the reference state. When the membrane is cooled down at t = 30s, the strains increase. During heating we observe an opposite trend in the strains. The duration heating voltage in the recovery step is 15 s, just long enough to go back to reference state. When we increase this duration, we observe slightly negative ε_{xx} and ε_{yy}.

Downloaded From: https://www.spiedigitallibrary.org/conference-proceedings-of-spie on 18 Jun 2023
Terms of Use: https://www.spiedigitallibrary.org/terms-of-use

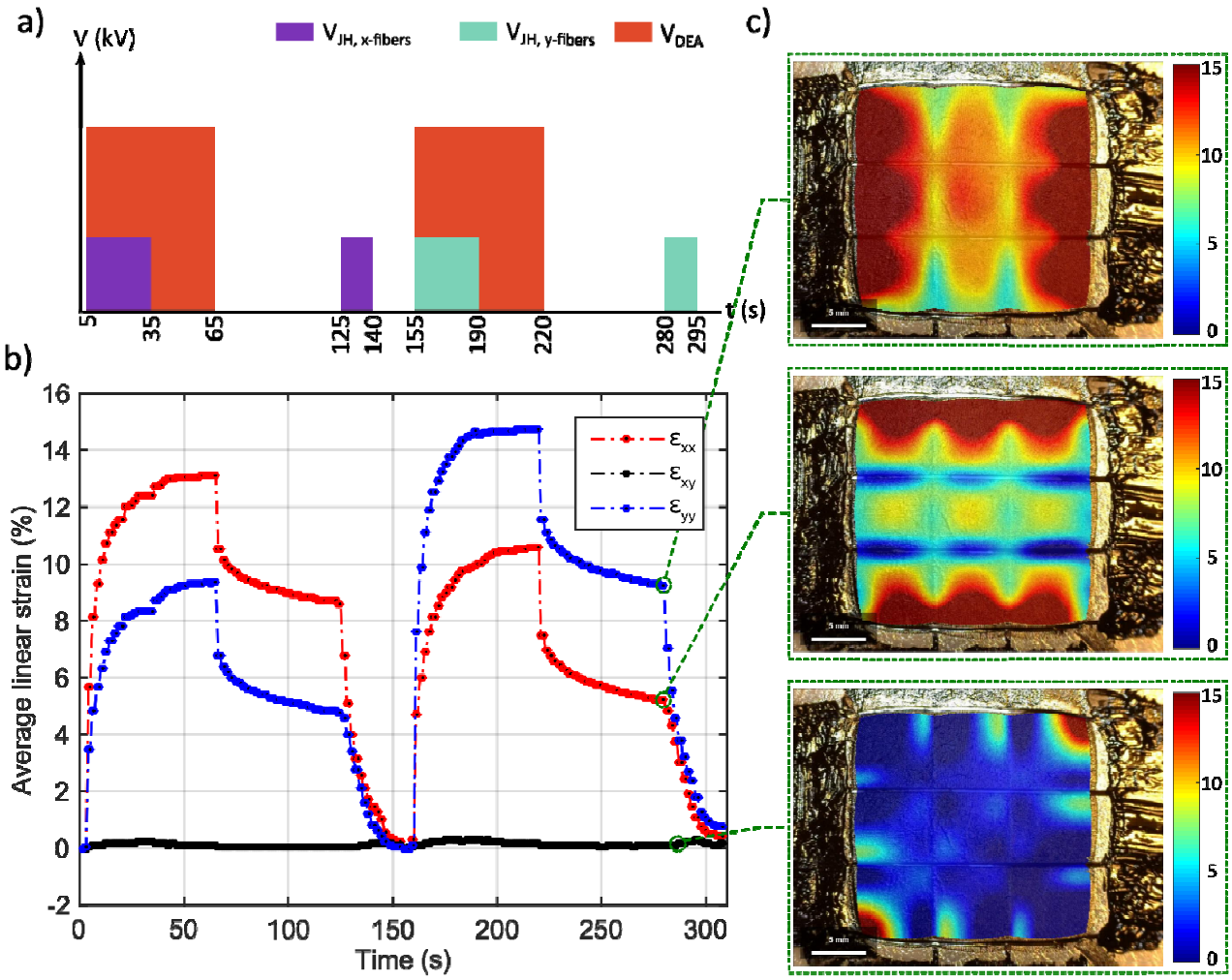

Figure 6. a) Time sequence of the actuation (HV) and Joule heating voltages for the device shown in Fig 1. b) The evolution of the measured in-plane strains when different fibers sets are sequentially heated and actuated. c) Mapping of strain components on active region at t = 280s.

After one minute of latching, the ratio of locked strains ($\varepsilon_{xx}/\varepsilon_{yy}$ or $\varepsilon_{yy}/\varepsilon_{xx}$) is 1.80. Compared to nylon or carbon fibers, SMP fibers perform poorly due undesired softening of unaddressed fiber set. To improve this ratio, we designed a plus shape DEA. We used only two SMP fibers that are oriented perpendicularly. The fibers have a uniform thickness of 75 µm. Their widths vary across their lengths: wider at the intersection (4.5 mm) and narrower at the outside of the overlap (750 µm). A schematic of this design is shown in the inset of Fig. 7a. The wider section of the fibers locally reduces the electrical resistance, thus reduces the heating power at this location. The inset of Fig. 7b shows the IR image when the horizontal fiber is heated. As seen in Fig. 7b, the temperature of the heated fibers drops from 70 °C to 42°C at the center where the temperature of the unaddressed fiber increases from 24 °C to 42 °C.

To actuate the device in the horizontal direction, we apply a heating voltage of 240 V to the horizontal fiber and actuate the DEA with a voltage of 3 kV. After 30 s, we remove the heating voltage and allow the membranes to cool for 30s. After the deformed shape is fixed by the SMP fiber, we remove the DEA voltage. The device is then kept latched for 1 minute. Finally, we heat the SMP fiber again to recover the locked strain. Fig. 7c shows how ε_{xx} and ε_{yy} evolve during these processes. As we partially solved the cross-heating issue, we are able to greatly increase the strain ratio. Figure 7d shows the strain ratio of $\varepsilon_{xx}/\varepsilon_{yy}$ during the DEA actuation in the *x*-direction. After 1 minute of latching, the strain ratio is approximately 8.

Downloaded From: https://www.spiedigitallibrary.org/conference-proceedings-of-spie on 18 Jun 2023
Terms of Use: https://www.spiedigitallibrary.org/terms-of-use

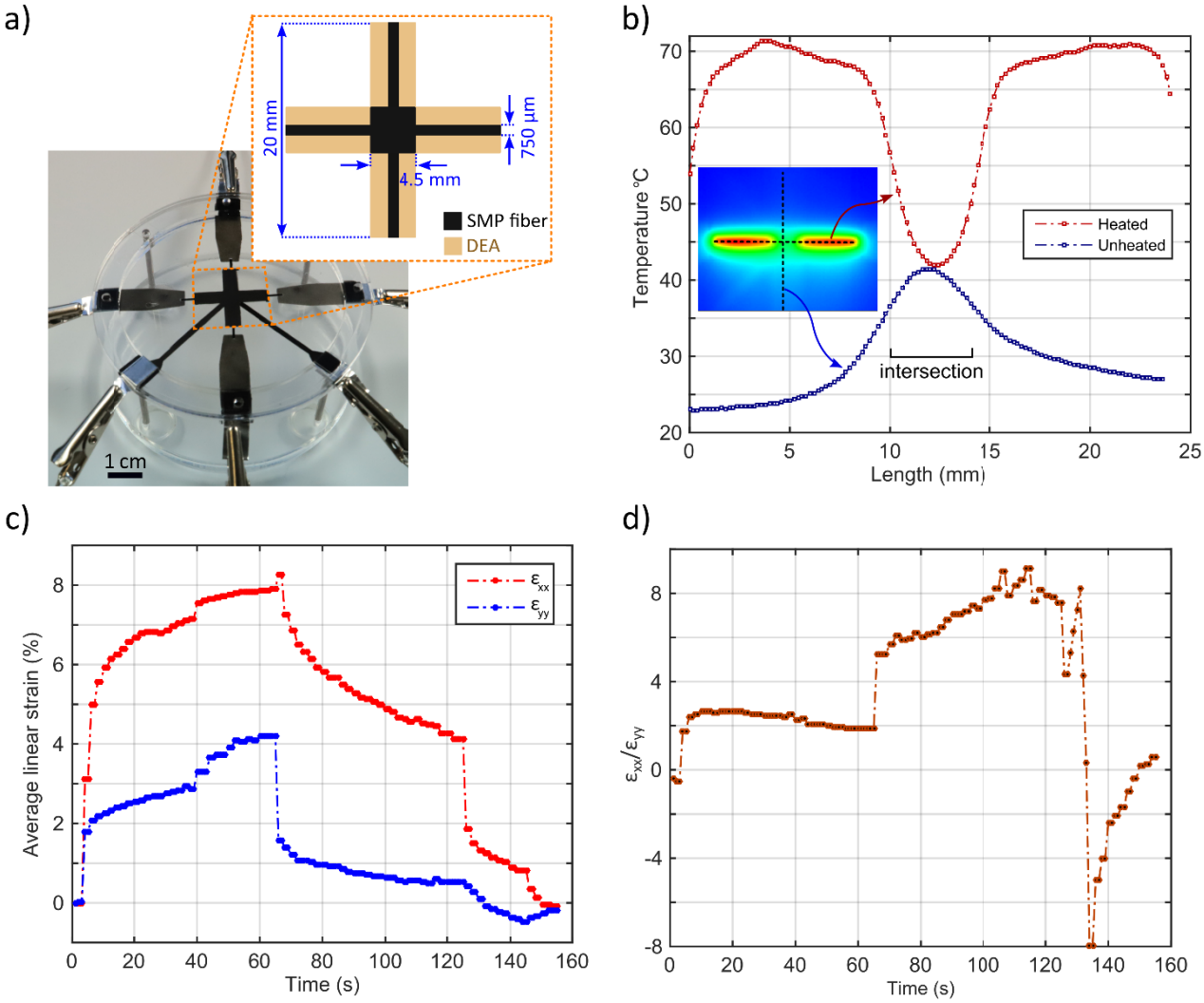

Figure 7. a) A photograph of a plus shape DEA with 2 embedded SMP fibers. b) The temperature distribution along the lengths of the heated (red) and the unheated (blue) fibers. The inset captures an IR image when the horizontal fiber is heated. c) The strains along the longitudinal direction of the heated and the unheated fibers. d) Evolution of the strain ratio for actuation in the *x*-direction, reaching a peak of over 8.

5. CONCLUSION AND OUTLOOK

We combined conductive SMP fibers with DEAs to introduce on-demand bi-directional actuation with latching ability. This is achieved by using two fiber sets aligned perpendicularly. The selection is made by softening one of these SMP fiber sets, which change their stiffness drastically within a small range of temperature increase. By increasing number of fiber sets and changing their orientations, it is possible to increase the degrees of freedom.

The assembled devices are alternately actuated in two perpendicular directions; the deformation in the direction of softened fibers are higher than the deformation in the transverse direction. Due to cross-heating between SMP fibers, the deformation along the stiff fibers are not completely blocked. Different design better decouple fiber heating and therefore improve asymmetrical actuation such as uniaxial deformation.

The method developed here can augment the degrees of freedom of dielectric elastomer actuators without the need of multiple high power supplies. This methodology can be implemented into bending structures, i.e. soft grippers, where

Downloaded From: https://www.spiedigitallibrary.org/conference-proceedings-of-spie on 18 Jun 2023
Terms of Use: https://www.spiedigitallibrary.org/terms-of-use

multi-degrees of freedom enabling more conformal wrapping of different objects. Combining soft actuation mechanisms with different shaped SMPs will enable us to morph planer membranes into more complex 3D structures and to keep the deformed shape in a power-free state. Origami-inspired reversibly foldable structures can also be obtained by spatially patterning SMP shapes and sequentially addressing them. By changing the order of heated SMPs, a completely different folding shape is achievable. Not only the location and the geometry of SMP affects the folding structure but also the sequence of addressing. This will allow a spatiotemporal shape control of stretchable surfaces.

ACKNOWLEDGMENTS

This work was supported by the Swiss National Science Foundation grant number 200020_165993. We thank S. Rosset at the University of Auckland for helpful discussions.

REFERENCES

[1] R. Pelrine, R. Kornbluh, Q. B. Pei, and J. Joseph, "High-speed electrically actuated elastomers with strain greater than 100%," *Science,* vol. 287, pp. 836-839, Feb 4 2000.
[2] T. Q. Lu, J. H. Huang, C. Jordi, G. Kovacs, R. Huang, D. R. Clarke*, et al.*, "Dielectric elastomer actuators under equal-biaxial forces, uniaxial forces, and uniaxial constraint of stiff fibers," *Soft Matter,* vol. 8, pp. 6167-6173, 2012.
[3] T. Q. Lu, Z. B. Shi, Q. Shi, and T. J. Wang, "Bioinspired bicipital muscle with fiber-constrained dielectric elastomer actuator," *Extreme Mechanics Letters,* vol. 6, pp. 75-81, Mar 2016.
[4] J. S. Huang, T. Q. Lu, J. Zhu, D. R. Clarke, and Z. G. Suo, "Large, uni-directional actuation in dielectric elastomers achieved by fiber stiffening," *Applied Physics Letters,* vol. 100, May 21 2012.
[5] Z. B. Yu, W. Yuan, P. Brochu, B. Chen, Z. T. Liu, and Q. B. Pei, "Large-strain, rigid-to-rigid deformation of bistable electroactive polymers," *Applied Physics Letters,* vol. 95, Nov 9 2009.
[6] X. F. Niu, X. G. Yang, P. Brochu, H. Stoyanov, S. Yun, Z. B. Yu*, et al.*, "Bistable Large-Strain Actuation of Interpenetrating Polymer Networks," *Advanced Materials,* vol. 24, pp. 6513-6519, Dec 18 2012.
[7] Y. Qiu, Z. Ren, W. Hu, C. Liu, and Q. B. Pei, "Bistable Electroactive Polymer with Sharp Rigid-to-Rubbery Phase Transition," *Electroactive Polymer Actuators and Devices (EAPAD),* vol. 9798, 2016.
[8] G. Kofod, M. Paajanen, and S. Bauer, "Self-organized minimum-energy structures for dielectric elastomer actuators," *Applied Physics a-Materials Science & Processing,* vol. 85, pp. 141-143, Nov 2006.
[9] B. O'Brien, E. Calius, S. Xie, and I. Anderson, "An experimentally validated model of a dielectric elastomer bending actuator," *Electroactive Polymer Actuators and Devices (EAPAD),* vol. 6927, 2008.
[10] S. Rosset, O. A. Araromi, J. Shintake, and H. R. Shea, "Model and design of dielectric elastomer minimum energy structures," *Smart Materials and Structures,* vol. 23, Aug 2014.
[11] S. Shian, K. Bertoldi, and D. R. Clarke, "Dielectric Elastomer Based "Grippers" for Soft Robotics," *Advanced Materials,* vol. 27, pp. 6814-+, Nov 18 2015.
[12] J. Shintake, B. Schubert, S. Rosset, H. Shea, and D. Floreano, "Variable Stiffness Actuator for Soft Robotics Using Dielectric Elastomer and Low-Melting-Point Alloy," *IEEE/RSJ International Conference on Intelligent Robots and Systems (IROS),* pp. 1097-1102, 2015.
[13] D. McCoul, S. Rosset, N. Besse, and H. Shea, "Multifunctional shape memory electrodes for dielectric elastomer actuators enabling high holding force and low-voltage multisegment addressing," *Smart Materials and Structures,* vol. 26, Feb 2017.
[14] X. F. Niu, P. Brochu, B. Salazar, and Q. B. Pei, "Refreshable Tactile Displays based on Bistable Electroactive Polymer," *Electroactive Polymer Actuators and Devices (EAPAD),* vol. 7976, 2011.
[15] S. Rosset, O. A. Araromi, S. Schlatter, and H. R. Shea, "Fabrication Process of Silicone-based Dielectric Elastomer Actuators," *Journal of Visualized Experiments,* Feb 2016.
[16] N. Besse, S. Rosset, J. J. Zarate, and H. Shea, "Flexible Active Skin: Large Reconfigurable Arrays of Individually Addressed Shape Memory Polymer Actuators," *Advanced Materials Technologies,* vol. 2, Oct 2017.

Downloaded From: https://www.spiedigitallibrary.org/conference-proceedings-of-spie on 18 Jun 2023
Terms of Use: https://www.spiedigitallibrary.org/terms-of-use

[17] B. Aksoy, N. Besse, R. J. Boom, B. J. Hoogenberg, M. Blom, and H. Shea, "Latchable microfluidic valve arrays based on shape memory polymer actuators," *Lab on a chip,* Jan 21 2019.
[18] A. Poulin, S. Rosset, and H. R. Shea, "Printing low-voltage dielectric elastomer actuators," *Applied Physics Letters,* vol. 107, Dec 14 2015.
[19] A. N. Gent, "A new constitutive relation for rubber," *Rubber Chemistry and Technology,* vol. 69, pp. 59-61, Mar-Apr 1996.
[20] J. S. Plante and S. Dubowsky, "Large-scale failure modes of dielectric elastomer actuators," *International Journal of Solids and Structures,* vol. 43, pp. 7727-7751, Dec 2006.
[21] X. H. Zhao and Z. G. Suo, "Method to analyze electromechanical stability of dielectric elastomers," *Applied Physics Letters,* vol. 91, Aug 6 2007.
[22] J. A. Zhu, H. Stoyanov, G. Kofod, and Z. G. Suo, "Large deformation and electromechanical instability of a dielectric elastomer tube actuator," *Journal of Applied Physics,* vol. 108, Oct 1 2010.
[23] S. Schlatter, P. Illenberger, and S. Rosset, "Peta-pico-Voltron: An open-source high voltage power supply," *HardwareX,* vol. 4, p. e00039, 2018/10/01/ 2018.
[24] J. Blaber, B. Adair, and A. Antoniou, "Ncorr: Open-Source 2D Digital Image Correlation Matlab Software," *Experimental Mechanics,* vol. 55, pp. 1105-1122, Jul 2015.
[25] G. A. Holzapfel, "Nonlinear Solid Mechanics: A Continuum Approach for Engineering Science," *Meccanica,* vol. 37, pp. 489-490, July 01 2002.

Downloaded From: https://www.spiedigitallibrary.org/conference-proceedings-of-spie on 18 Jun 2023
Terms of Use: https://www.spiedigitallibrary.org/terms-of-use